Polyhedron 29 (2010) 3324–3328

Contents lists available at ScienceDirect

Polyhedron

journal homepage: www.elsevier.com/locate/poly

Synthesis and characterization of two novel organic–inorganic hybrid solids from Keggin ions and metal coordination complexes

Yan-Fen Li [a], Dalton G. Hubble [a], Russell G. Miller [a], Hou-Yin Zhao [a], Wei-Ping Pan [a], Sean Parkin [b], Bangbo Yan [a,*]

[a] Department of Chemistry, Western Kentucky University, 1906 College Heights Blvd, Bowling Green, KY 42101, USA
[b] Department of Chemistry, University of Kentucky, Lexington, KY 40506-0055, USA

ARTICLE INFO

Article history:
Received 18 June 2010
Accepted 9 September 2010
Available online 24 September 2010

Keywords:
Polyoxometallate
Keggin cluster
Hydrogen bond
Tungsten
Iron
Cobalt

ABSTRACT

Two new hybrid compounds, $[Co(4,4'\text{-bpy})_2(H_2O)_4][(4,4'\text{-bpyH}_2]_2[CoW_{12}O_{40}]\cdot 8H_2O$ (**1**) and $[Fe(2,2'\text{-bpy})_3]_3[H_2W_{12}O_{40}]\cdot 6H_2O$ (**2**), (4,4′-bpy = 4,4′-bipyridine, 2,2′-bpy = 2,2′-bipyridine) have been hydrothermally synthesized. These solids were characterized by elemental analysis, thermogravimetric analysis, UV–Vis spectroscopy and X-ray diffraction. The hydrogen-bonding interactions in **1** lead to the formation of a three dimensional network consisting of $[CoW_{12}O_{40}]^{6-}$ anionic clusters, $[Co(4,4'\text{-bpy})_2(H_2O)_4]^{2+}$ cations and lattice water molecules, while the discrete Keggin ion $[H_2W_{12}O_{40}]^{6-}$ in compound **2** is surrounded by 14 $[Fe(2,2'\text{-bpy})_3]^{2+}$ complexes through CH···O interactions (2.24–2.56 Å).

1. Introduction

In the development of photocatalytic solid materials, the spatial arrangement of electron donor and acceptor species are critical to their efficient electron or energy transfer. In general, the approaches to the design and development of solid assemblies for solar energy conversion purposes are to adsorb molecular sensitizers onto the surface of wide-band gap semiconductors [1], or to incorporate photo-sensitizers into solid matrices such as zeolite [2] or mesoporous solids [3]. Our interest is to synthesize photocatalytic hybrid solid systems using molecular metal–organic complexes and polyoxometallates (POMs) as building units. POMs have drawn much attention as building blocks of supramolecular materials, especially of hybrid organic–inorganic systems [4–13]. Moreover, POMs have been studied for their photocatalytic properties in the reduction of water due to their similarities in properties to nano-sized semiconductor materials such as TiO_2 and ZnO. Some POMs, for example Keggin anions ($[MW_{12}O_{40}]^{n-}$, M = B, Si, Fe, Co, P; and $[H_2W_{12}O_{40}]^{6-}$) have shown photocatalytic properties for the production of hydrogen from water splitting [14–17]. However, these Keggin ions absorb only UV light, which consists of a small portion of solar energy. Thus, the use of visible light absorbing metal–organic complexes as sensitizers is necessary as they are expected to inject electrons into POMs through varies interactions such as hydrogen bonding, electrostatic interactions and coordination bonds. Recently, supramolecular complexes have been prepared in which the interacting components are associated by non-covalent interactions, in particular hydrogen bonding, and photoinduced energy-transfer has been observed between metalloporphyrins and hydrogen-bonded organic fragments [18,19]. As observed in the assembly of supramolecular chromophore–electron relay systems, the non-covalent bond interactions, such as metal–ligand coordination bonds and hydrogen bonding, not only have advantages in the syntheses, but also can mimic the natural photosynthetic assembly and provide electron transfer pathways [20]. In this respect, the study of the interactions between transition metal–organic complexes and POMs, and hence the donor–acceptor interactions in the solid state, can provide valuable information on their electronic properties and electron transfer properties. On the other hand, iron polypyridine complexes, such as $[Fe(2,2'\text{-bpy})_3]^{2+}$, have recently been studied as guests in zeolite cages [21–25]. Furthermore, it has been shown that Fe(II) polypyridyl complexes can be used as photosensitizers, and these would be potential alternatives to their ruthenium analoges in dye-sensitized solar cells [26–28]. To investigate the hydrogen bonding and electrostatic interactions between metal complexes with POMs in solid compounds and their photochemical properties, we set out to study the syntheses and properties of solid state materials containing Keggin cluster ions and metal polypyridyl complexes such as $[Fe(2,2'\text{-bpy})_3]^{2+}$, using Keggin clusters as starting materials. We selected $[CoW_{12}O_{40}]^{6-}$ and

* Corresponding author.
E-mail address: bangbo.yan@wku.edu (B. Yan).

0277-5387/$ - see front matter © 2010 Elsevier Ltd. All rights reserved.
doi:10.1016/j.poly.2010.09.015

$[H_2W_{12}O_{40}]^{6-}$ as our starting materials because of their interesting photochemical properties [14]. Herein, we reported the synthesis, characterization and properties of two new compounds, [Co(4,4′-bpy)$_2$(H_2O)$_4$][(4,4′-bpyH_2]$_2$[$CoW_{12}O_{40}$]·8H_2O (**1**) and ([Fe(2,2′-bpy)$_3$]$_3$[$H_2W_{12}O_{40}$]·6H_2O) (**2**).

2. Experiments

$K_6[CoW_{12}O_{40}]\cdot 16H_2O$ was prepared according to the literature method [29]]. All other chemicals were obtained from commercial sources and used without purification. UV–Vis diffusion reflectance spectra were recorded on a Varian Cary 100 UV–Vis spectrophotometer equipped with the DRA-CA-30 diffuse reflectance accessory. The infrared spectra were recorded from 400 to 4000 cm^{-1} on a Perkin Elmer Spectrum One FTIR spectrometer using KBr pellets. The thermogravimetric data were collected on a TA Q5000 TGA instrument. Powder X-ray analysis was performed on an ARL Thermo X-ray diffraction instrument.

2.1. Synthesis

Compound **1**, ([Co(4,4′-bpy)$_2$(H_2O)$_4$][4,4′-bpyH_2]$_2$[$CoW_{12}O_{40}$]·8H_2O), was synthesized hydrothermally from a mixture of 4,4′-bipyridine (0.16 g), $Co(CH_3COO)_2\cdot 4H_2O$ (0.06 g), $K_6[CoW_{12}O_{40}]\cdot 16H_2O$ (0.83 g) and water (5 mL). The mixture was transferred to a Teflon lined autoclave and heated at 120 °C for 2 days. After the autoclave was cooled to room temperature naturally, green crystals of **1** were filtered, washed with water, and dried in air (yield based on W: 65%). Elemental analysis: *calcd*. for $C_{20}H_{30}CoN_4O_{26}W_6$: C, 12.61; H, 1.59; N, 2.94; *Found*: C, 11.93; H, 1.84; N, 2.91%. IR (KBr pellet, cm^{-1}): 1636(m), 1617(s), 1493(m), 1412(m), 937(s), 879(s), 755(s). UV–Vis (powder, λ_{max}/nm): 255, 306, 630.

Compound **2**, ([Fe(2,2′bpy)$_3$]$_3$[$H_2W_{12}O_{40}$]·6H_2O), was synthesized using a similar method to that used for **1**. In a typical reaction, a mixture of 2,2′-bipyridine (2,2′-bpy, 0.037 g), iron(II) chloride tetrahydrate (0.015 g), $Na_6H_2W_{12}O_{40}$ (0.11 g) and water (3 mL) was transferred to a Teflon lined autoclave and heated at 120 °C for 2 days. After the autoclave was cooled to room temperature naturally, red crystals of **2** were filtered, washed with water, and dried in air (yield based on Fe: 51%). Elemental analysis: *calcd*. for $C_{90}H_{86}Fe_3N_{18}O_{46}W_{12}$: C, 23.86; H, 1.91; N, 5.57; *Found*: C, 22.98; H, 1.93; N, 5.61%. IR (KBr pellet, cm^1): 1637(m), 1605(s), 1468(s), 1446(s), 925(s), 874(s), 787(s). UV–visible (powder, λ_{max}/nm): 258, 288, 375, 520.

2.2. Crystallography

X-ray diffraction data for compounds **1** and **2** were collected at 90.0(2) K on a Nonius kappa CCD diffractometer. Raw data were integrated, scaled, merged and corrected for Lorentz-polarization effects using the HKL-SMN package [30]. The structures were solved by direct methods and refined against F^2 by weighted full-matrix least-squares calculations [31]. Hydrogen atoms of 4,4′-bpy or 2,2′-bpy were placed at calculated positions and refined using a riding model. No attempts were made to locate hydrogen atoms of water molecules from the difference maps. Non-hydrogen atoms were refined with anisotropic displacement parameters. Atomic scattering factors were taken from the International Tables for Crystallography [32]. Crystal data and relevant details of the structure determinations are summarized in Table 1 and selected geometrical parameters are given in Table 2.

Table 1
Crystal data and structure refinement for **1**–**2**.

	1	**2**
Formula	$C_{40}H_{60}Co_2N_8O_{52}W_{12}$	$C_{90}H_{86}Fe_3N_{18}O_{46}W_{12}$
Mol. wt.	3809.02	4529.50
Crystal system	Monoclinic	Monoclinic
Space group	*C*2/c	$P2_1/n$
a (Å)	21.2792(2)	18.5071(2)
b (Å)	15.2369(2)	26.1678(3)
b (Å)	20.0644(2)	22.2042(3)
α (°)	90	90
β (°)	106.5564(4)	93.0928(5)
γ (°)	90	90
V (Å^3)	7487.9(1)	10737.6(2)
Z	4	4
ρ (g cm^{-3})	3.383	2.801
μ (mm^{-1})	18.910	13.284
Wavelength (Å)	0.71073	0.71073
Temperature (K)	90(2)	293(2)
Reflections collected/unique [R_{int}]	76001/8567[0.0709]	195522/24526[0.1395]
Goodness-of-fit (F^2)	1.082	1.015
Final *R* indices [$I > 2\sigma(I)$]	R_1 = 0.0290, wR_2 = 0.0585	R_1 = 0.0504, wR_2 = 0.0948
R indices (all data)	R_1 = 0.0427, wR_2 = 0.0624	R_1 = 0.1096, wR_2 = 0.1146

Table 2
Selected interatomic distances (Å) in compounds ([Co(4,4,-bpy)$_2$(H_2O)$_4$][4,4-bpyH_2]$_2$[$CoW_{12}O_{40}$]·8H_2O (**1**) and ([Fe(2,2′bpy)$_3$]$_3$[$H_2W_{12}O_{40}$]·6H_2O (**2**).

	Compound **1**		Compound **2**	
	Range	Average	Range	Average
W–O_t	1.715(5)–1.724(4)	1.720	1.705(7)–1.742(8)	1.721
W–$O_{\mu 2}$	1.848(4)–2.045(4)	1.933	1.867(8)–1.996(7)	1.925
W–$O_{\mu 4}$	2.152(4)–2.173(4)	2.162	2.114(7)–2.286(7)	2.203
Fe(1)–N			1.939(9)–1.973(9)	
Fe(2)–N			1.950(9)–1.982(9)	
Fe(3)–N			1.933(11)–1.978(9)	
Co(1)–O	1.884(4)–1.890(4)			
Co(2)–O	2.100(5)–2.117(5)			
Co(2)–N	2.112(5)			

3. Results and discussions

Compounds **1**–**2** were synthesized using hydrothermal methods. The use of cluster compounds as starting materials is straight forward and the synthesis is easy to control. As expected, control of the pH of the reaction mixtures is critical for the crystallization of these compounds. Compound **1** can crystallize in a narrow pH range at around 7.5 and in a temperature range of 110–160 °C. At low pH (~5), compound **1** become a minor phase and a different compound is formed as the major phase. However, bad crystal quality precludes us from solving the structure. Compound **2** can be crystallized in the wide pH range of 3–8. The reaction temperature is also important to get good crystals. The optimal conditions for the preparation of compound **2** required adjustment of the solution pH to approximately 7 by addition of KOH.

3.1. Description of the structures

Single-crystal X-ray crystallographic analysis reveals that the structure of compound **1** consists of the anionic cluster $[CoW_{12}O_{40}]^{6-}$, lattice water molecules and the charge balancing cations $[4,4'\text{-bpy}H_2]^{2+}$ and $[Co(4,4\text{-bpy})_2(H_2O)_4]^{2+}$. The anionic unit, $[CoW_{12}O_{40}]^{6-}$, has the structure of the α-Keggin cluster [33], with a central tetrahedral cobalt atom surrounded by four groups of three edge-sharing octahedra (i.e. W_3O_{13} subunits), which are in

Table 3
Geometrical parameters of selected hydrogen bonds (Å, deg) for compound **1**.

D–H···A	d(D–H)	d(H···A)	d(D···A)	∠DHA
O1w–H1wa···O12#1	0.839	1.974	2.774	158.9
O2w–H2wa···O3w#1	0.844	1.858	2.701	178.2
O3w–H3wb···O18#2	0.844	1.952	2.788	170.1
O2w–H2wb···O5w	0.844	1.918	2.738	163.4
O5w···O16#3	0.853	2.050	2.772	141.9

D = donor, A = acceptor.
Symmetry transformations used to generate equivalent atoms: #1 $x + 1/2, y + 1/2, z$; #2 $-x + 1/2, y - 1/2, -z + 1/2$; #3 $-x + 1, y, -z + 1/2$.

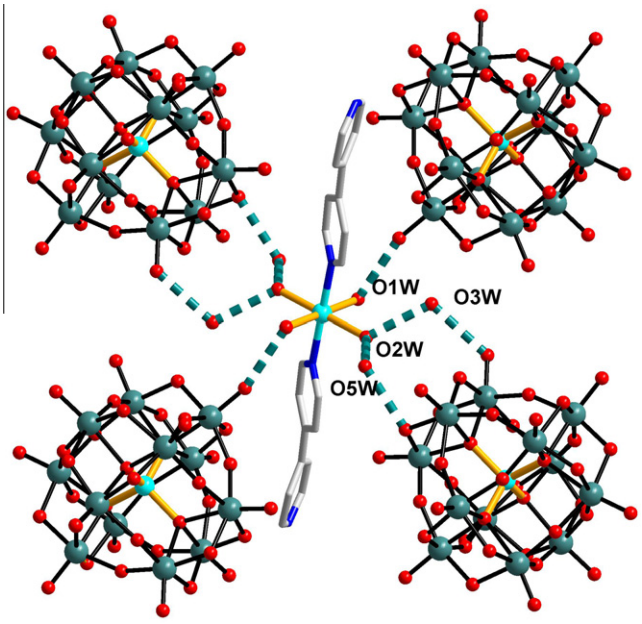

Fig. 1. Hydrogen bonds between $[CoW_{12}O_{40}]^{6-}$ anionic clusters, $[Co(4,4\text{-bpy})_2(H_2O)_4]^{2+}$ cations, and lattice water molecules in **1.**

turn linked to each other and to the central CoO_4 tetrahedron by shared oxygen atoms at the vertices. The central cobalt atom is coordinated to four oxygen atoms in a slightly distorted tetrahedral arrangement, with Co^{II}–O bonds distances of 1.884(4) and 1.890(4) Å. These bond lengths are comparable to those of the Co^{II}–O distances (1.895(12) Å) in $K_6[Co^{II}W_{12}O_{40}]\cdot 11H_2O$ [34], indicating the Co is 2+. The Co^{II}–O distances are, as expected, longer than Co^{III}–O (1.836(10) Å) in $K_6[Co^{III}W_{12}O_{40}]\cdot\sim 16H_2O$ [33]. As usual, the W–O bond lengths decrease with the decreasing coordination number of the oxygen atom, with values averaging 2.162(9) Å for four-coordination ($O_{\mu 4}$), 1.933(4) Å for two-coordination ($O_{\mu 2}$) and 1.720(5) Å for the terminal oxygen atoms (O_t) (see Table 2). Bond valence sum calculations indicate all W atoms have the oxidation 6+.

In the $[Co(4,4'\text{t-bpy})_2(H_2O)_4]^{2+}$ cation, the cobalt atom adopts an octahedral coordination geometry, bonded to four water molecules and two 4,4′-bpy ligands which are in *trans*- positions (bond lengths: Co–N 2.112(5); Co–O: $2.100(5) \times 2$, $2.167(5) \times 2$ Å). In this complex, the 4,4′-bpy molecule is acting as a monodenate ligand, using one of its nitrogen atoms to bond to cobalt. Terminal 4,4′-bpy ligands were also observed in another compound, $[Co_2(4,4'\text{-bpy})_6\ (W_6O_{19})_2]$ [35]. Based on charge balance, the second nitrogen atom of the 4,4′-bpy ligands should be protonated.

The presence of coordinated and lattice water molecules allows the formation of extensive hydrogen bonding within the solid structure of **1** (Table 3). As shown in Fig. 1, hydrogen bonds between $[CoW_{12}O_{40}]^{6-}$ anionic clusters, $[Co(4,4\text{-bpy})_2(H_2O)_4]^{2+}$ cations and lattice water molecules are observed in **1**. Hydrogen bonds are formed between the coordinated water molecule O(1w) and the terminal oxygen O(12) of the anion (O(1w)···O(12) 2.765 Å). Hydrogen bonds are also observed between lattice water molecules (O3w and O5w) and both coordinated waters (O2w) and terminal oxygens of the anion. Thus, each $[Co(4,4'\text{-bpy})_2(H_2O)_4]^{2+}$ cation is hydrogen bonded to four $[CoW_{12}O_{40}]^6$ anionic clusters. In turn, each $[CoW_{12}O_{40}]^{6-}$ anionic cluster links to four $[Co(4,4'\text{-bpy})_2(H_2O)_4]^{2+}$ cations. These hydrogen-bonding interactions lead to the formation of a three dimensional network consisting of $[CoW_{12}O_{40}]^{6-}$ anionic clusters,

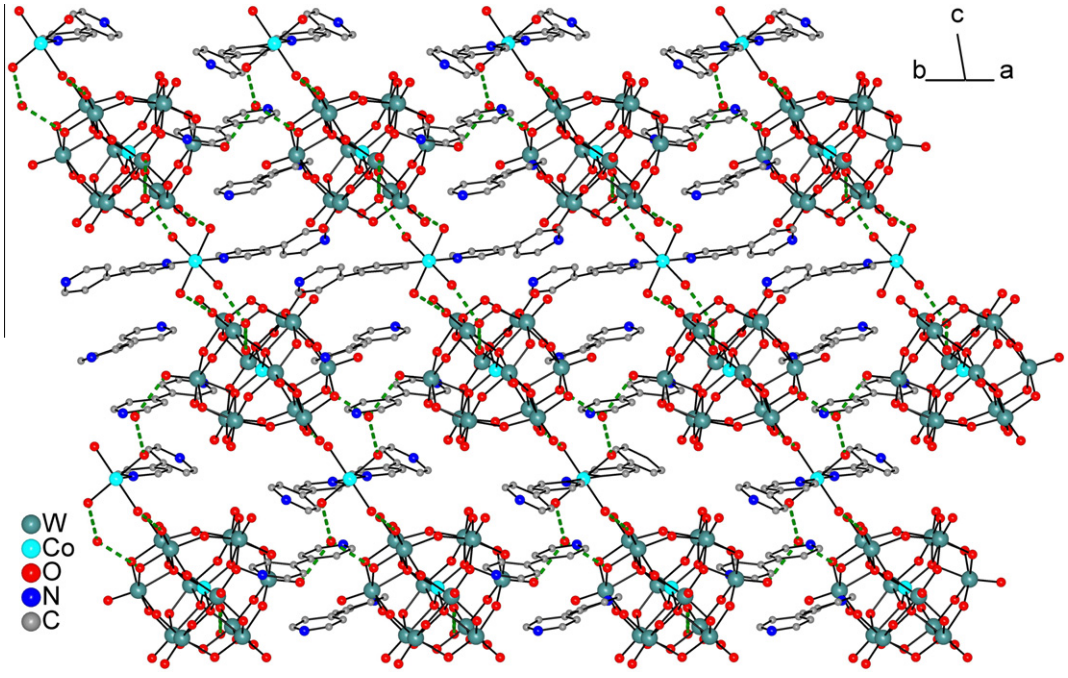

Fig. 2. 3D network consisting of $[CoW_{12}O_{40}]^{6-}$ anionic clusters, $[Co(4,4'\text{-bpy})_2(H_2O)_4]^{2+}$ cations and lattice water molecules in **1**.

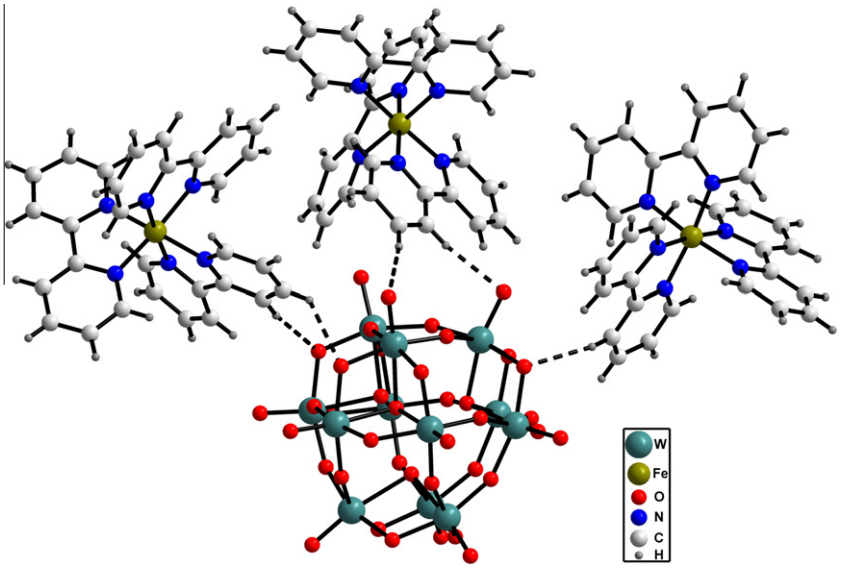

Fig. 3. Interactions between the $[Fe(2,2'\text{-bpy})_3]^{2+}$ complex and $[H_2W_{12}O_{40}]^{6-}$ in **2**.

$[Co(4,4'\text{-bpy})_2(H_2O)_4]^{2+}$ cations and lattice water molecules (Fig. 2). The $[Co(4,4'\text{-bpy})_2(H_2O)_4]^{2+}$ cation acts as square planar node and the anion as a seesaw node. The channels formed by the hydrogen bonding are occupied by the cation $[4,4'\text{-bpyH}_2]^{2+}$ and water molecules.

The crystal structure of compound **2** consists of $[H_2W_{12}O_{40}]^{6-}$ anions, $[Fe(2,2'\text{bpy})_3]^{2+}$ cations and lattice water molecules. Similar to the Keggin cluster in compound **1**, the cluster $[H_2W_{12}O_{40}]^6$ in **2** consists of four groups of tri-metallic $\{(WO_6)_3\}$ units. Each (WO_6) octahedron in a tri-metallic unit shares an edge with a neighboring one, and the $\{(WO_6)_3\}$ units link together via corner sharing WO_6 octahedra to form a cluster cage. There are three unique Fe(II) cations in the asymmetric unit. Each displays a distorted octahedral coordination sphere, coordinated to three 2,2′-bpy ligands as shown in Fig. 3. All three unique iron complexes are chiral and have the same conformation, being Δ isomers.

Even though there are no "classical hydrogen bonds" between the $[Fe(2,2'\text{-bpy})_3]^{2+}$ complex and the Keggin ion $[H_2W_{12}O_{40}]^6$ in **2**, there are several CH···O contacts in the range 2.24–2.56 Å between these units (Table 4). These interactions play a significant role in the assembly of these ions into a solid. With these CH···O contacts, each Keggin anion is surrounded by 14 $[Fe(2,2'\text{-bpy})_3]^{2+}$ units (Fig. 4), while each $[Fe(2,2'\text{-bpy})_3]^{2+}$ unit is surrounded by four Keggin anions. These non-covalent interactions not only help to hold the two types of fragments together, but also to direct the arrangement of these building units in the 3D space. The calculated bond valence sum for all W atoms is averaged at +6.09 (from the range 5.94–6.29).

3.2. UV–Vis spectra

The UV–Vis diffuse reflectance spectra of **1**–**2** are shown in Fig. S1. Both compounds show broad bands around 250–300 nm, which can be attributed to ligand-to-metal charge-transfer (LMCT) transitions (O → W) of the Keggin anions [17]. The broad band at 540–680 nm for **1** could be attributed to metal-to-ligand (d–π) charge-transfers (MLCT) and d–d transitions of cobalt.

The spectrum of compound **2** exhibits a very broad MLCT band centered at around 520 nm [36],[37]], showing a red shift in comparison to the spectrum of $Fe(bpy)_3SO_4$ which exhibits a MLCT band at 486 nm. This alteration in the absorption spectra can be attributed to the interaction between $[Fe(bpy)_3]^{2+}$ and the cluster $[H_2W_{12}O_{40}]^6$ anions through CH···O contacts.

Table 4
Geometrical parameters of selected hydrogen contacts(Å, deg) for compound **2**.

D–H···A	d(H···A)	d(D···A)	∠DHA
C(18)–H(18)···O(34)#1	2.37	3.0720	132
C(23)–H(23)···O(27)	2.53	3.2679	137
C(24)–H(24)···O(21)	2.30	3.2235	169
C(27)–H(27)···O(29)#1	2.56	3.3346	141
C(35)–H(35)···O(14)#2	2.27	3.0336	139
C(45)–H(45)···O(10)#3	2.52	3.4220	163
C(65)–H(65)···O(11)#4	2.43	3.3399	168
C(66)–H(66)···O(25)#4	2.37	3.2940	170
C(72)–H(72)···O(14)#5	2.25	3.1130	155
C(75)–H(75)···O(27)#6	2.47	3.2062	136
C(76)–H(76)···O(26)#6	2.41	3.2689	154
C(78)–H(78)···O(35)#7	2.42	3.2450	148
C(85)–H(85)···O(3)#7	2.51	3.3602	152
C(86)–H(86)···O(7)#7	2.50	3.3375	149

D = donor, A = acceptor.
Symmetry transformations used to generate equivalent atoms: #1: $-1/2+x, 1/2-y, 1/2+z$; #2: $1/2+x, 1/2-y, -1/2+z$; #3: $-x,1-y,-z$; #4: $1+x,y,z$; #5: $1/2-x,1/2+y,1/2-z$; #6: $1-x,1-y,1-z$; #7: $1/2+x,1/2-y,1/2+z$.

3.3. TG analysis

The thermal stability of compounds **1** and **2** was investigated on powder samples in a nitrogen atmosphere in the temperature range 40–700 °C. The TG plot (Fig. S2) of compound **1** shows a weight loss of 5.2% from 30 to 200 °C, which is attributed to the loss of water molecules (calcd 5.68%). The weight loss of 17.2% in the temperature range 250–600 °C corresponds to the decomposition of 4,4′-bpy molecules. Compound **2** (Fig. S2) shows a weight loss of 2.47% up to 125 °C, which is attributed to the loss of water molecules (calcd 2.39%), followed by a weight loss of 30.4% at 150–700 °C, which corresponds to the decomposition of 2,2′-bpy ligand molecules (calcd 31.1%).

4. Conclusions

Two novel hybrid compounds containing Keggin clusters and transition metal complexes have been hydrothermally synthesized

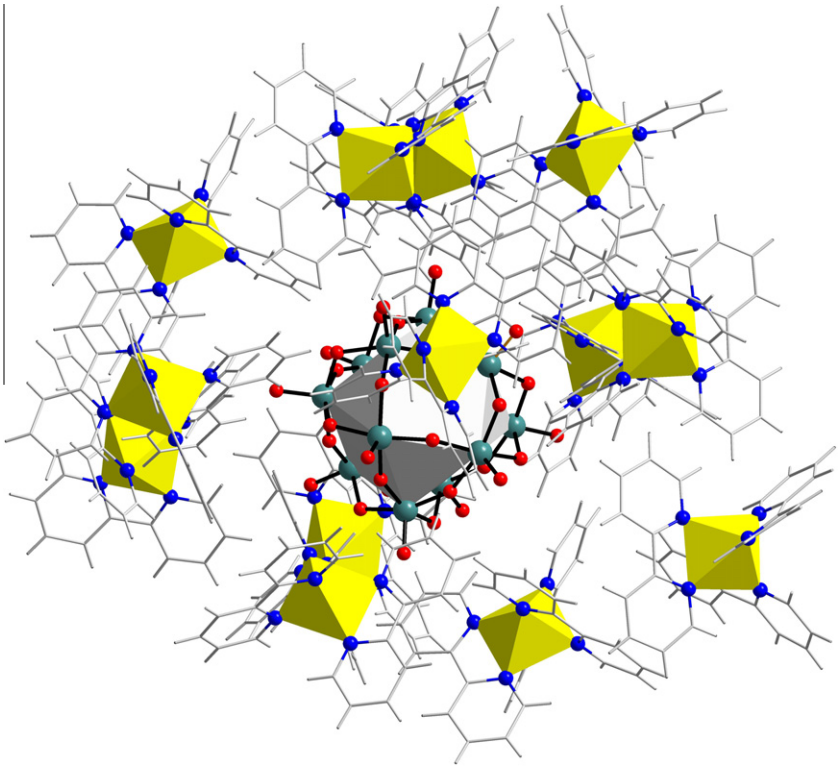

Fig. 4. A view of the Keggin anion $[H_2W_{12}O_{40}]^6$ surrounded by $[Fe(2,2'\text{-bpy})_3]^{2+}$ units in **2**.

and structurally characterized. The successful isolation of compounds **1** and **2** demonstrates that the hydrothermal method can be used for the incorporation of photosenitizers such as $[Fe(bpy)_3]^{2+}$ into solid compounds to form hybrid materials. The non-covalent interactions play an important role in the assembly of the building blocks into solids. They direct the arrangement of these building units in the 3D space and the formation of 3D structures. This provides an alternative method for the synthesis of multi-component photoactive systems for energy transfer or charge separation to conventional methods using covalent bond interactions. Studies are underway to investigate the photocatalytic properties of these novel solids.

Acknowledgements

Financial support of this work by the Kentucky EPSCoR (RSF-030-06), the WKU start-up grant and the WKU PIF is greatly appreciated.

Appendix A. Supplementary data

CCDC 781651 and 781652; contains the supplementary crystallographic data for **1** and **2**. These data can be obtained free of charge via http://www.ccdc.cam.ac.uk/conts/retrieving.html, or from the Cambridge Crystallographic Data Centre, 12 Union Road, Cambridge CB2 1EZ, UK; fax: (+44) 1223-336-033; or e-mail: deposit@ccdc.cam.ac.uk. Supplementary data associated with this article can be found, in the online version, at doi:10.1016/j.poly.2010.09.015.

References

[1] B. O'Regan, M. Grätze, Nature 353 (1991) 737.
[2] P.K. Dutta, M. Ledney, Prog. Inorg. Chem. 44 (1997) 209.
[3] Y. Diskin-Posner, S. Dahal, I. Goldberg, Angew. Chem., Int. Ed. 39 (2000) 1288.
[4] R. Nandini Devi, Eric Burkholder, Jon Zubieta, Inorg. Chim. Acta 348 (2003) 150.
[5] B. Yan, Y. Xu, X. Bu, N.K. Goh, L.S. Chia, G.D. Stucky, J. Chem. Soc., Dalton Trans. (2001) 2009.
[6] B. Yan, N.K. Goh, Lian S. cHIA, Inorg. Chim. Acta. 357 (2004) 490.
[7] B. Yan, Yan-Fen Li, Hou-Yin Zhao, Wei-Ping Pan, Sean Parkin, Inorg. Chem. Commun 12 (2009) 1139.
[8] M. Wei, C. He, W. Hua, C. Duan, S. Li, Q. Meng, J. Am, Chem. Soc. 128 (2006) 13318.
[9] S. Reinoso, P. Vitoria, L. Lezama, A. Luque, J.M. Gutierrez-Zorrilla, Inorg. Chem. 42 (2003) 3709.
[10] P.-Q. Zheng, Y.-P. Ren, L.-S. Long, R.-B. Huang, L.-S. Zheng, Inorg. Chem. 44 (2005) 1190.
[11] Chun.-Mei. Wang, Shou.-Tian. Zheng, Guo.-Yu. Yang, Inorg. Chem. 46 (2007) 616.
[12] J. Wang, P. Ma, Y. Shen, J. Niu, Cryst Growth Des. 8 (2008) 3130.
[13] H. Jin, Y. Qi, E. Wang, Y. Li, X. Wang, C. Qin, S. Chang, Cryst. Growth Des. 6 (2006) 2693.
[14] R. Akid, J.R. Darwent, J. Chem. Soc., Dalton Trans. (1985) 395.
[15] Y. Li, C. Ren, S. Peng, G. Lu, S. Li, J. Molec, Catal. A: Chem. 246 (2006) 212.
[16] T. Yamase, R. Watanabe, J. Chem. Soc., Dalton Trans. (1986). 1699–1678.
[17] J.R. Darwent, J. Chem. Soc. Chem. Commun. (1982) 798.
[18] J.L. Sessler, B. Wang, A. Harriman, J. Am. Chem. Soc. 117 (1995) 704.
[19] P. Tecilla, R.P. Dixon, G. Slobodkin, D.S. Alavi, D.H. Waldeck, A.D. Hamilton, J. Am. Chem. Soc. 112 (1990) 9408.
[20] M.D. Ward, Chem. Soc. Rev. 26 (1997) 365.
[21] K. Mori, K. Kagohara, H. Yamashita, J. Phys. Chem. C 112 (2008) 2593.
[22] G. Sewell, R.J. Forster, T.E. Keyes, J. Phys, Chem. A 112 (2008) 880.
[23] Y. Umemura, Y. Minai, T. Tominaga, J. Phys, Chem. B 103 (1999) 647.
[24] A. Vargas, A. Hauser, L.M.L. Daku, J. Chem. Theory Comput. 5 (2009) 97.
[25] V. Ganesan, R. Ramaraj, Langmuir 14 (1998) 2497.
[26] S. Ferrere, Chem. Mater. 12 (2000) 1083.
[27] S. Ferrere, B.A. Gregg, J. Am. Chem. Soc. 120 (1998) 843.
[28] J.E. Monat, J.K. McCusker, J. Am. Chem. Soc. 122 (2000) 4092.
[29] A.L. Nolan, R.C. Burns, G.A. Lawrance, J. Chem. Soc., Dalton Trans. (1998) 3041.
[30] Z. Otwinowski, W. Minor, Methods in enzymology, in: C.W. Carter Jr., R.M. Swet (Eds.), Macromolecular Crystallography part A, vol. 276, Academic Press, USA, 1997, pp. 307–326.
[31] G.M. Sheldrick, Acta Crystallogr., Sect. A64 (2008) 112.
[32] International Tables for Crystallography, vol C, Th. Hahn (Ed.) Kluwer Academic Publishers, Holland.
[33] A.L. Nolan, C.C. Allen, R.C. Burns, D.C. Craig, G.A. Lawrance, Aust. J. Chem. 53 (2000) 59.
[34] N. Casañ-Pastor, P. Gomez-Romero, G.B. Jameson, L.C.W. Baker, J. Am. Chem. Soc. 113 (1991) 5658.
[35] L. Zhang, Y. Wei, C. Wang, H. Guo, P. Wang, J. Solid State Chem. 177 (2004) 343.
[36] M. Cheng, W. Ma, C. Chen, J. Yao, J. Zhao, Appl. Catal. B 65 (2006) 217.
[37] S.J. Hug, S.G. Boxer, Inorg. Chim. Acta (1996) 323.